

# Analytical Study of 5G Beamforming in the Reactive Near-Field Zone

Maryna Nesterova<sup>1</sup>, Stuart Nicol<sup>2</sup>

<sup>1</sup> System Development, Aprel Inc, Kanata, Canada, MarynaN@aprel.com

<sup>2</sup> Aprel Inc, Kanata, Canada, StuartN@aprel.com

**Abstract**—An innovative method of assessment of the non-zero phase shift between electric ( $E$ ) and magnetic ( $H$ ) field vectors is introduced, making possible an analysis of the impact on wave propagation of a 5G array antenna. The presented two-probe measurement technique is based on a robust assessment of spatial distribution of  $E$  and  $H$  fields along with a signal propagation orientation in the reactive near-field zone of a device. This method allows one to quantify both the energy radiating outward into free space and the reactive portion of the reversing electromagnetic field which affects the efficiency of the transmitter. The ability to examine the Poynting vector variation relative to the changing phase of 0, 30, and 90 degrees between two active elements of the array antenna provides information about beam strength and direction of propagation. This method elucidates the effect of the phase shift on wave propagation direction, back-scattering, and power density.

**Index Terms**—antenna, 5G, millimetre-wave propagation, near-field measurement, beamforming, reactive near-field, power density.

## I. INTRODUCTION

In the reactive near-field zone the electric and magnetic fields are not synchronized in phase and change orientation very rapidly with distance from a signal source in all radial directions. Numerical simulations can't account for this complex phenomenon, resulting in poor accuracy and significant underestimation of the power density in close proximity to the antennas. The benefit of measuring the phase shift between  $E$  and  $H$  fields of a signal directly is in seeing a real-time field transformation which doesn't require any field-reconstruction calculations or simulations.

APREL has developed an automated measurement system for near-field measurements of both  $E$  and  $H$  components (Fig. 1). The 5G probes are of a low Q broad band antenna type which utilize a scientifically developed sensor arrangement, allowing for high sensitivity and directivity detection of tested fields. Due to the specific geometry of the 5G-probe design, solderless connectors, and passive path, perturbation with reactive near fields is minimized. This effect is accounted for during the probe calibration procedure through the evaluation of coupling loss with a non-resonating co-planar micro stripline. The fields can be measured at a closest distance of 0.5mm from a device surface with a grid resolution of 0.05mm. This

precision is especially important for frequencies over 60GHz.

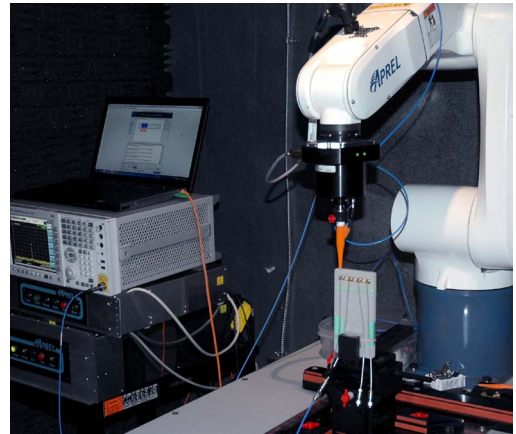


Fig. 1. EM-ISight automated measurement system for near-field scanning.

## II. TWO-PROBE METHOD DESCRIPTION.

### A. Poynting Vector in Near-Field Zone

The authors propose using a two-probe measuring technique to take measurements of projections of electric and magnetic field vectors on test planes at assorted distances over a device. The post-processing RF-ISight application provided allows for the analysis of phase, directivity, and beamforming along with calculations of the power density of 5G signals.

Within the two-probe method procedure, the  $E$  and  $H$  probes take measurements at every point of a chosen test grid, rotating 360° to detect the radial flux orientation of the corresponding fields (Fig. 2).

This method allows for the calculation of energy propagation as the cross product of the electric field vector  $\vec{E}$ , and the magnetic field vector  $\vec{B}$ . The conventional industry method, based as it is on impedance approximation from far-field measurements, is unreliable in near-field evaluations when the efficiency of the circuit has to be determined, as evidenced by [1]. Instead, in the proposed method, the Poynting vector is employed in combination with the measured electric and magnetic field directivity data

in order to construct the energy propagation vector, as follows.

In free space, as in a vacuum, magnitude of the magnetic field density vector  $\vec{B}$  is proportional to  $H$  by the familiar formula:

$$B = \mu_0 H \quad (1)$$

where  $B$  is magnetic flux density ( $T$ ) and  $\mu_0$  is the magnetic constant ( $H/m$ ). Unless specified otherwise, the terms *magnetic field* and *magnetic field vector* are used to refer to  $H$ . The Poynting vector theorem represented as:

$$\vec{S} = \frac{1}{\mu_0} \vec{E} \times \vec{B} \quad (2)$$

where  $\vec{S}$  is the power density vector ( $\text{W/m}^2$ ), is shown in [2].

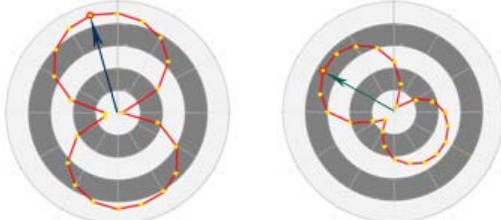


Fig. 2. Polar chart of  $E$  (left) and  $H$  (right) fields measured 360° at a single point of the test grid with a spacing of 15°. Vectors for maximum amplitude are indicated with arrows.

### B. Direction of Power Propagation

In the near-field region, signal propagation is shaped by the complexity of the phase relationship between  $E$  and  $H$ : the electric and magnetic fields have a phase shift  $\theta'$ . As a result there is no EM wave propagation close to a device, and the field oscillations are unstable [3]. Should an angle  $\theta'$  occur (measured counter-clockwise from  $\vec{E}$ ) between the direction of the maximum electric field  $\vec{E}$  and the direction of maximum magnetic field  $\vec{B}$  vectors, the latter is projected perpendicular to the electric field vector as seen in Fig. 3. Thus, (2) is modified to become

$$\vec{S} = E_{max} H_{max} \cos(\theta') \hat{n} \quad (3)$$

where scalars  $E_{max}$  and  $H_{max}$  are maximum measured magnitudes of electric and magnetic fields respectively,  $\hat{n}$  is the unit vector normal to both electric and magnetic vectors, and  $\theta'$  is the phase shift. In cases when angle  $\theta$  is greater than 180 degrees the Pointing vector reverses its direction.

As described in [4], an angle of exactly 180 degrees represents the standing wave condition when energy is not propagating. This event was observed at the half-wavelength distance over a horn antenna. Further studies of this phenomenon are progressing.

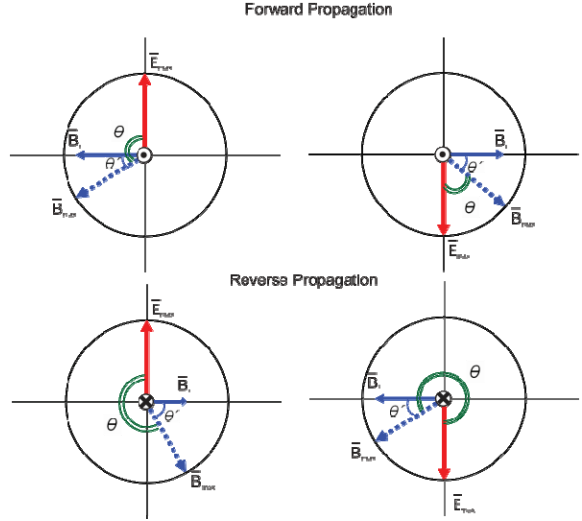


Fig. 3. The four possible arrangements of electric  $E$  and magnetic  $B$  field vectors resulting in energy propagation in freespace (top) moving out of the page, and (bottom) moving into the page, respectively. Note the projection of the measured magnetic field is perpendicular to  $\vec{E}_{max}$ .

## III. EXPERIMENTAL DATA

### A. Test Setup

Dealing with the millimetre-wavelength electric and magnetic field vectors in close proximity to resonating elements requires high precision in probe positioning and centering because the vector directions rapidly change within a very small space. It is important to consider the phase shift between  $E$  and  $H$  fields as a significant contributor to the backscattering effect. Thus, the grid size, resolution step, and rotational resolution are all factors of the fundamental frequency.

For this study, two elements of the array antenna were set to transmit 5G K<sub>a</sub> band signals with different phase, these being: synchronized, 30 degrees, and 90 degrees. The distance between elements was  $\pi\lambda$ , for wavelength  $\lambda$ . The  $E$  and  $H$  fields were measured at distances of  $\lambda/2$ ,  $\lambda$ , and  $2\lambda$ .

### B. Field Distribution in Reactive Zone

The post-processed test results are presented as a plot for maximum measured amplitude at every point of the grid with directional pointers indicating the maximum amplitude vector orientation measured by rotating the probe.

Both  $E$  and  $H$  field distribution plots demonstrated that synchronized waves are not merging even at a  $2\lambda$  distance, creating two independent beams with one element dominating over another (see column 1 of Fig. 4 and 5).

For the 30-degree phase test case, the  $E$  and  $H$  field distribution also showed the same signal dominance, although the field patterns were slightly different for the suppressed beam (see column 2 of Fig. 4 and 5).

In the 90-degree phase case the field distribution patterns have changed noticeably. Both fields created one hot spot at  $2\lambda$  (see column 3 of Fig. 4 and 5).

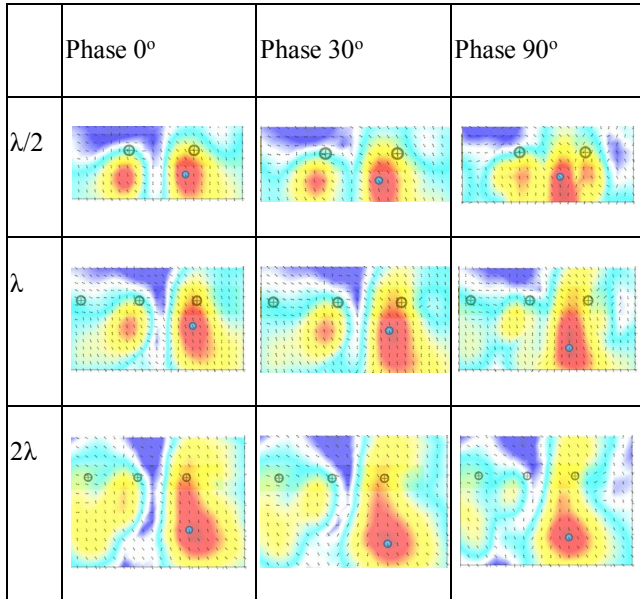


Fig. 4.  $E$  field distribution for 0-, 30-, and 90-degree phase at  $\lambda/2$ ,  $\lambda$ , and  $2\lambda$  separation distance from the DUT. Antenna elements are marked with a circled plus.

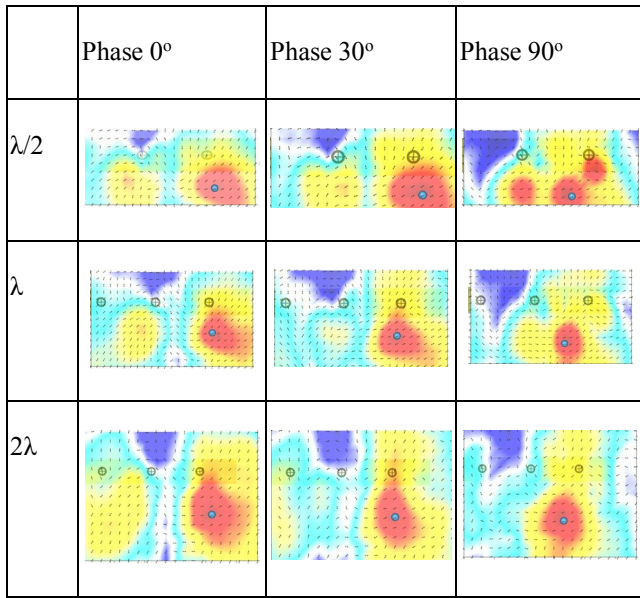


Fig. 5.  $H$  field distribution for 0-, 30-, and 90-degree phase at  $\lambda/2$ ,  $\lambda$ , and  $2\lambda$  separation distance from the DUT.

The blue marker on each plot indicates the maximum measured peak point of the field on the test plane. The

location of peak points for  $E$  and  $H$  fields are different for all tested cases.

Basic resonance effect is characterized by the 90-degree phase shift between electric and magnetic fields. As a result, in the reactive zone a location of the  $E$  and  $H$  peaks are spatially distinct.

### C. Peak Points Amplitude Comparison

At every tested level over the DUT the amplitude was normalized to the maximum measured at phase 0, as shown in Fig. 6, 7, and 8. For the closest measured distance of  $\lambda/2$  both electric and magnetic fields deviate depending on the phase between the antenna elements. The maximum  $E$  field is measured in the case of the zero phase while maximum  $H$  field is observed for a 90° phase (Fig. 6).

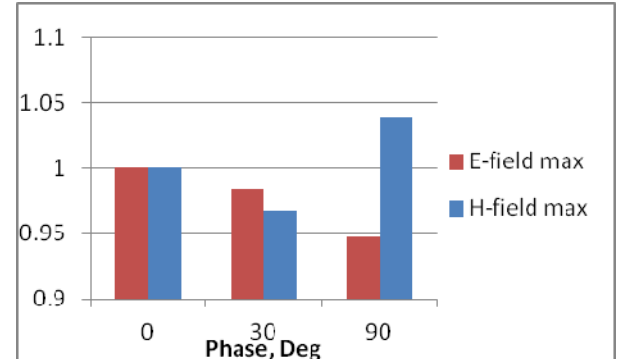


Fig. 6. Normalized maximum amplitude at  $\lambda/2$  distance over the DUT.

For the layer at a distance of one wavelength  $\lambda$  both  $E$  and  $H$  fields exhibit maxima for phase zero (Fig. 7).

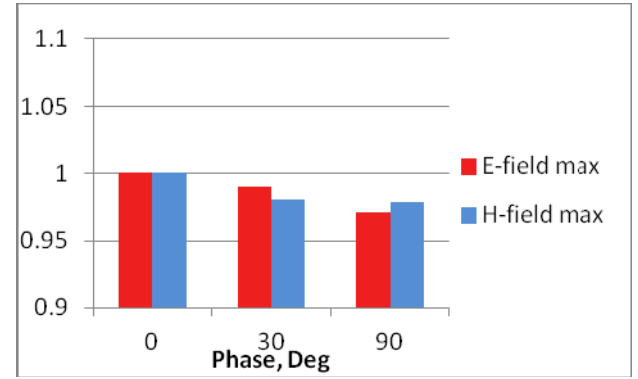


Fig. 7. Normalized maximum amplitude at  $\lambda$  distance over the DUT.

At the distance of  $2\lambda$  the maximum field amplitudes are almost the same for all three phase cases (Fig. 8).

Therefore, the well-established field-reconstruction technique, based as it is on the back-propagation principles using far-field measurements of either the  $E$  or  $H$  component of a propagating wave, cannot accurately evaluate the processes in the region closer than  $2\lambda$  to a signal source.

Furthermore, for reactive space closer than  $\lambda$ , measuring only the  $E$  or  $H$  field is not enough for the accurate reconstruction of the behavior of the Poynting vector and propagating power.

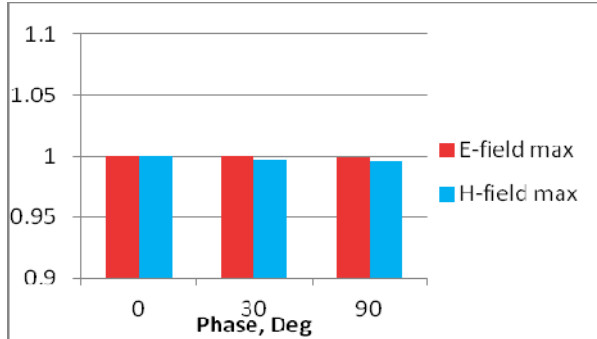


Fig. 8. Normalized maximum amplitude at  $2\lambda$  distance over the DUT.

#### D. Phase Shift between Electric and Magnetic Vectors

The method suggested by the authors provides a unique prospect to actually measure the reactive near-field with consideration of the  $E$  and  $H$  phase shift. While an evaluation surface can have different spatial orientations and shouldn't be flat, the probes measure only the orthogonal projections on the measurement surface.

The phase-shift indicators (Fig. 9) show the angle, assuming that the zero phase shift is directed vertically to the top of the plot.

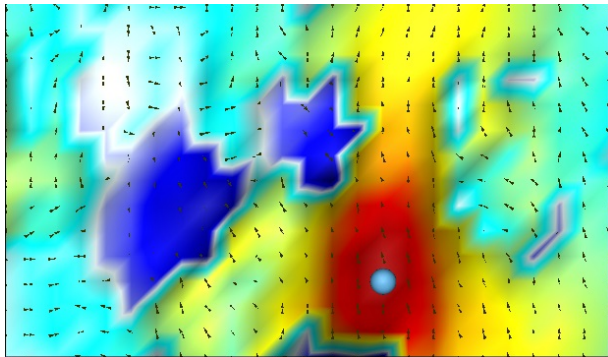


Fig. 9. Power density plot with phase shift indicators for test case of  $90^\circ$  phase between antenna elements measured at distance  $\lambda$ .

It is observed that for all test cases the phase shift in the hot-spot area is less than 15 degrees, although at other regions of the plot different angles are detected. This observation demonstrates that methods based on the assumption of a zero phase shift between  $E$  and  $H$  are deceptive, as they are unable to provide correct representation of the near field in close proximity to the circuit.

## IV. POWER DENSITY

### A. Back-Scattering Effect

One of the advantages of the two-probe method is an ability to evaluate the direction of the Poynting vector within the reactive zone based on measured phase shift between maximum amplitude vectors of electric and magnetic fields. The negative value of the Poynting vector represents the amount of energy propagating backwards.

In this study the power density direction is evaluated for all three test cases. The results presented in 3D format are shown in Fig. 10.

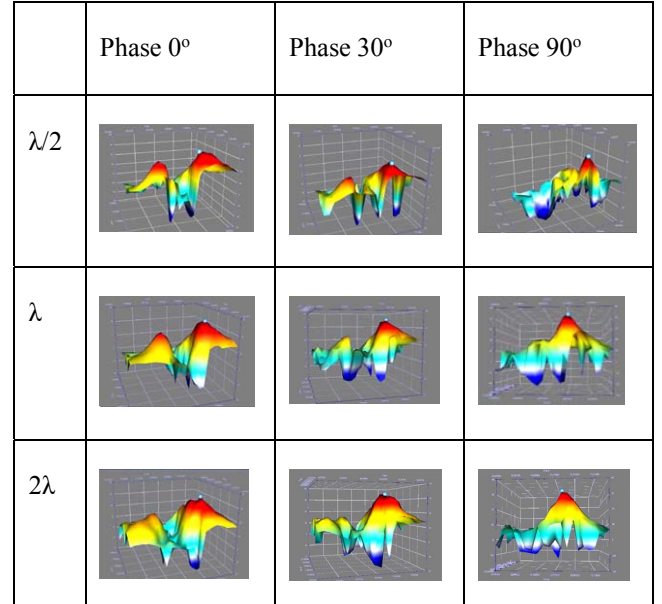


Fig.10. Poynting vector distribution for 0-, 30-, and 90-degree phase at  $\lambda/2$ ,  $\lambda$ , and  $2\lambda$  separation distance from the DUT.

On the colour scale of the presented plots, the negative Poynting vector corresponds to the dark blue end of the colour spectrum. The anti-peaks of the back-propagating energy have different geometry and spatial location for different test cases. Even at the  $2\lambda$  distance some reactive power is observed in values of 17% for Phase 0, 12% for phase  $30^\circ$ , and 9% for phase  $90^\circ$ .

Thus, the phase between elements is affecting the antenna performance. The two-probe method allows for precise evaluation of back-scattering and back-coupling effects.

### B. Power Density Comparison

During the analysis of data it became clear that considerations needed to be made for two different types of power density analyses: directional and isotropic. Directional power density (PD Dir) represents the maximum Poynting vector value, which is not averaged over time. The radial averaged (RMS) fields for every test point within the

measured grid defined the isotropic power density results (PD Iso) without phase shift consideration.

The presented power density values are normalized to the maximum PD Dir for the synchronized phase. Fig. 11, 12, and 13 exhibit substantial differences between maximum directional and isotropic power density results at all spatial levels. Such observations should be considered when determining the field strength or power density of a specific circuit designed for commercial use.

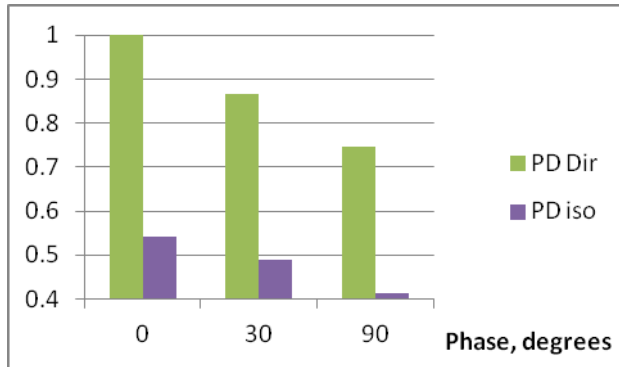


Fig. 11. Normalized maximum power density at  $\lambda/2$  distance over the DUT.

Close to the antenna, the peaks of both PD Dir and PD Iso vary considerably from case to case (Fig. 11), while further in space, at a distance of  $\lambda$ , the isotropic PD is consistent for all three phase cases (Fig. 12). However, at a separation of  $2\lambda$  the PD Iso slightly deviates, showing higher values for the  $90^\circ$  phase (Fig. 13).

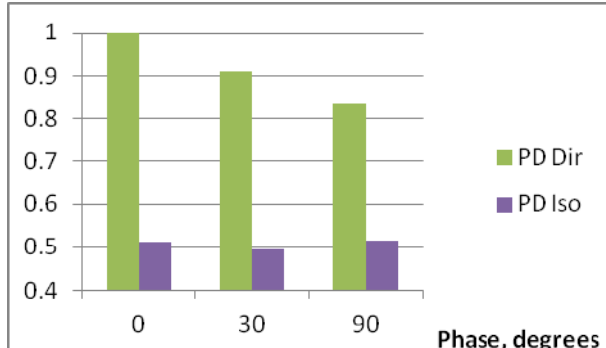


Fig. 12. Normalized maximum power density at  $\lambda$  distance over the DUT.

It was observed that PD Dir peaks are consistently highest for the phase 0 test events at all separation distances.

These results demonstrate the influence of the phase relationship between electric and magnetic components on the signal.

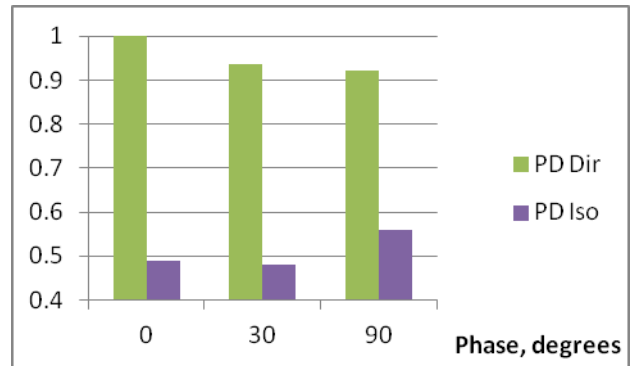


Fig. 13. Normalized maximum power density at  $2\lambda$  distance over the DUT.

## V. CONCLUSIONS

The complexity of the near-field region increases for 5G frequencies because of the non-zero phase shift between electric and magnetic oscillations. Due to the erratic nature of energy propagation in the near field (consult [5] for a robust analysis), the far-field measurements and back-propagation calculation methods are unable to evaluate adequately the electromagnetic field fluctuations in the reactive zone.

The characteristics of the near-field zone vary not just for different types of transmitters, but also for different setups of the same antenna, as demonstrated in this study. The proposed two-probe method provides the essential data for an analytical assessment of a 5G device for:

- Phase shift between  $E$  and  $H$  fields
- Field distribution and scattering
- Pointing vector spatial orientation
- Backscattering
- Signal propagation and directivity
- Power density.

High-frequency signals are directional and the beam forming process in the reactive zone must be considered. This will ultimately influence the efficiency of a circuit and the ability of the propagating fields to deliver the throughput desired. Where not all energy is delivered into freespace, it will ultimately impact the circuit. As such, signal integrity or similar attributes may cause problems in the aptness of the design to deliver the data output needed.

## References

- [1] T. Lecklider, "The world of the near field," Evaluation engineering, vol 44, p. 52, October 2005.
- [2] D. J. Griffiths, "Introduction to Electrodynamics," Prentice-Hall, Inc., September 1999, pp. 347-405.
- [3] I. Straus, "Near and far fields – from statics to radiation," Conformity, February 2001, [www.conformity.com/0102reflections.html](http://www.conformity.com/0102reflections.html).
- [4] M. Nesterova, S. Nicol, Y. Nesterova, "Two-probe method for advanced EM wave propagation analysis," IEEE RADIO 2017 International Conference, September 2017.
- [5] D. Brooks, S. Nicol, J. Hones, J. Lee, "Near-Field Magnetic Probe Method Predicting Far-Field Measurements," Progress in Electromagnetics Research Symposium, March 2013.